JOURNAL OF CATALYSIS 134, 479–491 (1992)

Quantitative Structural Analysis of Dispersed Vanadia Species in TiO_2(Anatase)-Supported V_2O_5

GREGORY T. WENT, LI-JEN LEU, AND ALEXIS T. BELL

Center for Advanced Materials, Lawrence Berkeley Laboratory, and Department of Chemical Engineering, University of California, Berkeley, California 94720

Received May 29, 1991; revised October 24, 1991

V_2O_5–TiO_2(anatase) catalysts have been studied under oxidizing and reducing conditions using *in situ* laser Raman spectroscopy (LRS) and temperature-programmed reduction (TPR) and oxidation (TPO). Quantitative Raman and TPO analysis of the oxidized samples show that these materials are comprised of a distribution of monomeric vanadyls, polymeric vanadates, and crystallites of V_2O_5. At low loadings, the predominant species are monomeric vanadyls, with the remaining vanadia being present in the form of polymeric vanadates. As the surface concentration of V_2O_5 increases, a maximum in the concentration of the polymeric vanadates is detected. Crystallites of V_2O_5 form at the expense of the polymeric vanadates as the loading is raised above the dispersive capacity of the TiO_2(anatase) support. An equilibrium polymerization model is proposed to account for the observed concentration of vanadia species, which leads to an initial polymer size of ~2 at low loadings, consistent with the formation of dimeric species. Raman and TPR/TPO studies of the reduction process indicate that the terminal V=O groups of the monomeric and polymeric vanadia species are removed preferentially to the bridging oxygen atoms of the polymeric species. The maximum loss of oxygen upon reduction is one oxygen atom per vanadium atom.

INTRODUCTION

Titania-supported V_2O_5 catalysts are used industrially for the partial oxidation of hydrocarbons and for the selective catalytic reduction (SCR) of NO with NH_3. In both of these applications, the optimal activity and selectivity is achieved when approximately one monolayer of vanadia is dispersed on the anatase phase of TiO_2 (*1–6*). These observations have provided motivation for investigations of the structure and distribution of the dispersed VO_x species and their influence on the catalytic properties of these materials (*6–11, 13*).

The structure of highly dispersed VO_x species present on the surface of fully oxidized TiO_2-supported V_2O_5 catalysts has recently been characterized using *in situ* infrared (IR), Raman (LRS), and ^{51}V NMR spectroscopies. Busca and co-workers (*7, 8*) and Went *et al.* (*9*) have shown that for low concentrations of V_2O_5, monomeric vanadyls are the primary species present on TiO_2 supports. This species is characterized by a narrow peak near 1030 cm^{-1} in both the IR (*7, 8*) and Raman (*9, 10*) spectra, indicative of a very strong V=O bond. ^{51}V NMR studies support this assignment and suggest that the monomeric species contains a fourfold coordinated vanadium with symmetry greater than twofold (*11*). As the vanadia loading increases, new Raman bands appear in the region of 800–1000 cm^{-1}, attributable to the terminal V=O bonds of polymeric vanadia species (*9*). The Raman band associated with the V=O groups of this species shifts to higher energy as the vanadia loading increases, indicating an increase in both the average vanadium coordination and the molecular weight of the polyvanadate species (*12*). In agreement with this interpretation, ^{51}V NMR spectroscopy shows an increase in the vanadium coordi-

0021-9517/92 $3.00

nation from fourfold to sixfold as the loading of vanadia increases (*11*). Vanadia loadings above a monolayer result in the appearance of crystalline V_2O_5 (*8–11, 13*).

The present paper reports the results of Raman spectroscopy and temperature-programmed reduction (TPR) and oxidation (TPO) experiments on a series of TiO_2(anatase)-supported V_2O_5 catalysts. The purpose of this work is to determine the distribution of vanadia species as a function of V_2O_5 loading and to determine the structural and compositional changes experienced by the dispersed species upon reduction.

EXPERIMENTAL

The gases used in this study were helium (Airco, 99.9995%), nitrogen (Matheson UHP grade, 99.995%), oxygen (Matheson Grade), and hydrogen (Matheson UHP grade, 99.995%). Mixtures of 1% O_2/He and 4% H_2/He used in the TPR and TPO experiments were obtained from Matheson.

The anatase phase of TiO_2, referred to hereafter as TiO_2(a), was obtained from $Ti(OH)_4$ formed by addition of titanium isopropoxide (Tyzar, Dupont) to a 1 : 1 water–isopropanol mixture at 268 K. After washing the solid several times to remove the isopropanol, it was dried in vacuum at 383 K overnight, then heated to 773 K in O_2 for 4 h. The phase of the resulting material was determined by LRS and X-ray diffraction to be ~95% anatase and ~5% brookite, with no detectable quantities of rutile. Chemical analysis placed the concentration of Fe, K, Cl, and Na impurities at <50 ppm.

Vanadia was introduced onto the support by incipient wetness impregnation with a solution of vanadium oxalate, as described in Ref. (*14*). Ammonium metavanadate (Aldrich Gold, 99.99%) was added slowly to a stoichiomeric amount of oxalic acid (Aldrich Gold, 99+%) at 353 K until all of the solid dissolved. The deep blue solution was diluted to the point needed to impregnate the support to incipient wetness (1 ml/g TiO_2(a)). The impregnated samples were dried in N_2 overnight at 383 K, calcined for 4 h in O_2 at 473 K, and then calcined for an additional 4 h at 73 K. The weight loadings of V_2O_5 were determined by X-ray fluorescence of the K_β X rays of vanadium, with titanium serving as the internal standard. The BET surface area of each sample was determined by static N_2 adsorption at 77 K.

Details of the Raman apparatus and calibration procedures are described in Ref. (*9*). Prior to acquisition of the Raman spectra, the samples were first calcined at 773 K for 1 h in flowing O_2, cooled to 373 K, then purged for 1 h in flowing He. For the reduction studies, H_2 was introduced at 373 K, then the sample was heated to the desired temperature and held at this temperature for 1 h. The sample was cooled to 373 K to stop the reduction process and to minimize the effects of thermal broadening of the Raman lines. Spectra were recorded between 200 and 1400 cm^{-1} with a resolution of 6 cm^{-1}, using the 488.0-nm line of an argon ion laser (Spectra Physics Model 165). The laser power at the sample was 50 mW. The collection time per scan, chosen near the saturation limit of the detector, ranged from 0.01 to 500 s, and multiple scans were collected for a total time of ~1000 s. After collection of the Raman spectra, the intense TiO_2(a) background occurring in the region of 700–1200 cm^{-1} was subtracted from each spectrum using the following procedure. First, each spectrum was normalized to the intensity of the 520 cm^{-1} band of the TiO_2(a) support. Next, the sloping background was removed by fitting the intensity of the first and last 50 points to a fourth-order polynomial, which was then subtracted from the data. The identical procedure was applied to the spectrum of the TiO_2(a) support, which was subsequently subtracted from the spectra of the V_2O_5/TiO_2(a) samples, to remove any remaining contribution from TiO_2(a).

TPR and TPO experiments were carried out in a quartz microreactor connected to a flow manifold. The effluent from the microreactor was analyzed by a quadrupole mass spectrometer (UTI Model 100C). Samples

were first pelletized into small particles (30–60 mesh) then loaded into the quartz reactor, which contains a porous frit to support the catalyst. The mass of the sample was chosen to maintain ~85 μmol of vanadium in the reactor. Calcination at 773 K for 1 h in 100 cm^3/min of pure O_2 preceded each TPR/TPO experiment. After cooling to 298 K, the TPR experiment was carried out by flowing a 4% H_2/He mixture at 20 cm^3/min through the reactor which was heated at 20 K/min to 773 K, and then held at this temperature until the H_2 consumption was complete. The sample was then cooled in He to 298 K, and followed immediately by a TPO experiment. Oxidation was carried out in a 1% O_2/He mixture fed at 20 cm^3/min. The temperature was raised at 20 K/min from 298 to 773 K, and held at 773 K until the oxidation was complete.

RESULTS AND DISCUSSION

Catalyst Characterization

Table 1 lists the vanadia loading (determined by X-ray fluorescence), BET surface area, and the surface vanadia density (expressed as micromoles of V_2O_5 per square meter) of the catalysts used in this study. A substantial increase in the surface density of V_2O_5 is observed as the loading is increased from 1.3 to 9.8 wt% V_2O_5. Comparison of the vanadia surface density for the titania-supported catalysts with that for the (010) plane of crystalline V_2O_5 suggests that the monolayer capacity is exceeded in the 9.8% sample. A decrease in the BET surface area is also observed as the vanadia loading increases.

TABLE 1

Catalyst Characteristics

Weight loading % V_2O_5[a]	BET surface area (m^2/g)	Surface density (μmol V_2O_5/m^2)
1.3	79	0.88
2.5	84	1.65
3.0	78	2.12
6.1	44	7.60
9.8	28	19.2
V_2O_5[b]	—	7.97

[a] Determined by XRD to ±6%.
[b] (010) plane of crystalline V_2O_5.

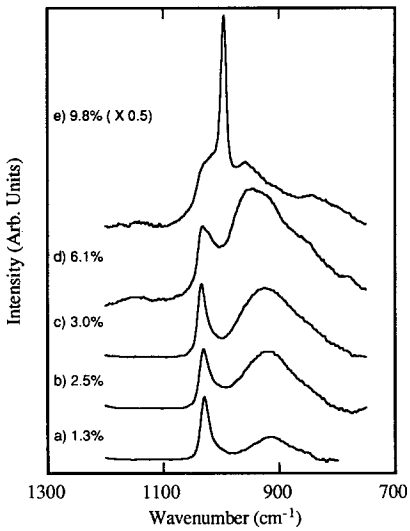

FIG. 1. Raman spectra of TiO_2(a)-supported V_2O_5, taken in dry He at 373 K, after calcination at 773 K: (a) 1.3% V_2O_5/TiO_2(a); (b) 2.5% V_2O_5/TiO_2(a); (c) 3.0% V_2O_5/TiO_2(a); (d) 6.1% V_2O_5/TiO_2(a); and (e) 9.8% V_2O_5/TiO_2(a). The intensities are scaled to the vanadia loading. Spectra are displayed following background subtraction over the region of 700–1200 cm^{-1}. Intensities are normalized to the vanadia loading for each sample.

LRS: Oxidized Catalysts

In situ Raman spectra of the freshly oxidized TiO_2(a)-supported V_2O_5 catalysts are shown in Fig. 1. Spectrum(a) for the 1.3% V_2O_5/TiO_2(a) sample exhibits a narrow peak at 1030 cm^{-1} and a broadband centered at 915 cm^{-1}. With increasing V_2O_5 loading, the intensity of the broad feature increases relative to the narrow band, which remains at 1030 cm^{-1}. In the spectra of the 2.5 and 3.0% V_2O_5/TiO_2(a) samples, a shoulder appears on the low-wavenumber side of the broad peak centered at ~925 cm^{-1}. This feature is clearly evident in the Raman spectra recorded for the 6.1 and 9.8% V_2O_5 loadings (Figs. 1d and 1e). The broad set of fea-

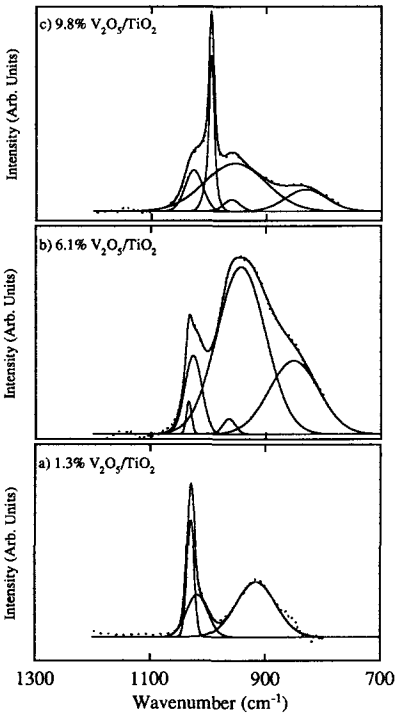

FIG. 2. Gaussian deconvolution of the Raman spectra shown in Fig. 1: (a) 1.3% V_2O_5/TiO_2(a); (b) 6.1% V_2O_5/TiO_2(a); and (c) 9.8% V_2O_5/TiO_2(a).

tures extending from 750 to 1000 cm^{-1} can be deconvoluted into three Gaussian peaks, as shown in Fig. 2. The first is centered near 840 cm^{-1} and does not shift appreciably in position with increasing V_2O_5 loading. A

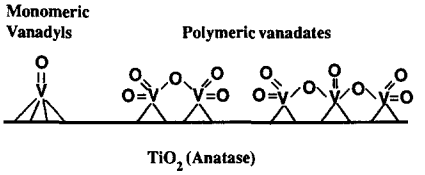

FIG. 3. Schematic depicting the structures of dispersed VO_x species.

second peak is located at 920 cm^{-1} in the spectrum of the 2.5% V_2O_5/TiO_2(a) sample and shifts to 955 cm^{-1} as the loading is increased to 9.8%. The third peak, which appears in the spectra of the 6.1 and 9.8% samples, is located at 960 cm^{-1} and is much narrower than the band located at 955 cm^{-1}. The spectrum of the 9.8% V_2O_5/TiO_2(a) sample exhibits an intense, narrow line at 997 cm^{-1}, characteristic of crystalline V_2O_5 (*15*). A summary of band positions determined by deconvolution of the Raman spectra is presented in Table 2.

The Raman line located at 1030 cm^{-1} in spectra(a)–(e) of Fig. 1 has been attributed to a monomeric vanadyl species bound directly to the TiO_2(a) support (*7, 9, 10*). This assignment is supported by the similarity of the position and width of this band to that observed for vanadium oxytrihalides ($VOBr_3$, $VOCl_3$, and VOF_3) (*16*). In Fig. 3, the monomeric species is depicted with four

TABLE 2

Summary of Raman Peak Locations

Weight loading % V_2O_5	Monomer (cm^{-1}) ν(V=O)[a]	ν(V–O–V)	Polymer (cm^{-1})	
			ν(V=O)[b]	ν(V=O)[c]
1.3	1030	—	915	—
2.5	1030	840	920	—
3.0	1032	850	930	—
6.1	1032	850	940	960
9.8	1028	830	955	960

[a] V=O stretch of monomeric vanadyl species.
[b] V=O stretches of dioxo vanadium groups at the ends of polymeric species.
[c] V=O stretch of vanadyl groups internal to polymeric species.

V–O–Ti bonds to the supports. The number of bonds anchoring the vanadyl group to the support cannot be determined from the Raman spectra; however, NMR studies indicate that the symmetry of this species is greater than twofold (*10*). The surface of anatase exposes primarily (001) planes, which contain two distinct fourfold oxygen arrangements comprised of separate Ti–O–Ti bridging oxygen atoms and Ti–O terminal oxygen atoms (*14*). The prevalence of this structure argues in favor of V–O bonds (of order <1) to four equivalent surface oxygen atoms giving rise to a species with C_{4v} symmetry. The distance between adjacent O atoms in this configuration (3.78 Å) (*17*) compares well with the Cl–Cl distance of $VOCl_3$ (3.54 Å) (*18*).

Closer inspection of the spectra in Fig. 1 indicates that the peak located at 1030 cm^{-1} broadens significantly as the V_2O_5 loading increases. The results of Gaussian deconvolution in Fig. 2 show that this feature is fit best to two peaks: a narrow component located at ~1030 cm^{-1} and a broader peak at located at slightly lower energy. The contribution of the broad peak increases steadily as the vanadia loading is raised and is the sole contribution to this feature in the spectrum of the 9.8% sample. This trend suggests that the narrow peak that dominates the spectrum of the 1.3% sample is associated with isolated vanadyl groups on the surface, whereas the broad peak arises from vanadyl species, which are in close proximity to each other on the surface.

The remaining features in Fig. 1 in the region of 700–1000 cm^{-1} have been assigned to polymeric vanadates (*9*). This assignment is based on the similarity in the position of the bands in this region with those for terminal V=O bonds of polyvanadate anions in solution (*12*). As the number of vanadium centers in the polyvanadates increases, the number of terminal V=O groups per vanadium decreases to accommodate V–O–V linkages. This results in a shift in the frequency of the remaining V=O bonds from ~900 to ~1000 cm^{-1} (*12*). A similar shift to higher frequency is observed in the Raman spectra of TiO_2(a)-supported V_2O_5 shown in Fig. 1. In the spectrum of 1.3% V_2O_5–TiO_2(a), the peak located at 915 cm^{-1} is assigned to the terminal V=O stretches of polyvanadte species. The location and width of this band suggest that it arises from the symmetric and asymmetric stretches of dioxo-vanadium centers. These pairs of modes are not well resolved in the spectra of numerous dioxo-vanadium compounds, including $[HV_2O_7]^{3-}$ (915, 905 cm^{-1}) (*12*), $[(VO_3)_n]^{n-}$ (945, 905 cm^{-1}) (*12*), and $K_3[VO_2F_2]$ (928, 890 cm^{-1}) (*19*). With increasing vanadia loading, the location of the dioxo-band shifts from 915 to 955 cm^{-1}. The magnitude of this shift is similar to that observed for the polymerization of $[HV_2O_7]^{3-}$ to $[(VO_3)_n]^{n-}$ in solution (*12*). The narrow feature located at 960 cm^{-1} in the spectra of the 6.1 and 9.8% V_2O_5/TiO_2(a) samples may be associated with vanadyl groups within the polyvanadate chains, as the location and width of this feature are similar to the those observed for vanadyl stretches of the two-dimensional polyvanadate ion $[V_{10}O_{28}]^{6-}$ (990, 960 cm^{-1}; FWHM ~15 cm^{-1}) (*12*). Finally, the band near 840 cm^{-1} can be attributed to the V–O–V bending vibrations in the polyvanadate species, given the similarity of the position of this band to that observed in $[HV_2O_7]^{3-}$ and $[V_{10}O_{28}]^{6-}$ ions, which exhibit bands at 810 and 840 cm^{-1}, respectively (*12*). A schematic of the proposed dimeric and trimeric species is shown in Fig. 3.

Quantitative Analysis of LRS

The distribution of different vanadia species can be determined from the Raman spectra shown in Fig. 1. To do so, we assume that the intensity of the scattered radiation measured at the detector can be expressed as

$$I_M = N_M \times \sigma_M \times \eta \times F$$

$$I_P = N_P \times \sigma_P \times \eta \times F$$

$$I_{TiO_2} = N_{TiO_2} \times \sigma_{TiO_2} \times \eta \times F, \quad (1)$$

where I_M is the intensity of monomeric peak for a given sample, N_M is the concentration of monomeric species in the sample, σ_M is the scattering cross section of the monomeric species, η is the scattering efficiency (No. counts detected/No. photons scattered), and F is the incident flux to the illuminated volume. Similar definitions apply to the polymeric species and the TiO_2(a) support. As defined, the scattering efficiency accounts for variations that occur from sample to sample due to color changes and to the alignment of the optics. The scattering cross sections are assumed to be solely a function of the molecular species and do not vary from sample to sample. If the vanadia overlayer is thin, then the penetration depth of incident radiation into the TiO_2(a) (and hence N_{TiO_2}) should be constant. Ratioing the intensities for the monomeric and polymeric species by the intensity for TiO_2(a) gives

$$I'_M = N_M \times \sigma'_M$$
$$I'_P = N_P \times \sigma'_P, \qquad (2)$$

where the normalized intensities and scattering cross sections are defined as

$$I'_M = \frac{I_M}{I_{TiO_2}}$$

$$I'_P = \frac{I_P}{I_{TiO_2}}$$

$$\sigma'_M = \frac{\sigma_M}{N_{TiO_2} \times \sigma_{TiO_2}}$$

$$\sigma'_P = \frac{\sigma_P}{N_{TiO_2} \times \sigma_{TiO_2}}. \qquad (3)$$

For each sample, in the absence of crystalline V_2O_5, a mass balance on vanadium gives

$$N = N_M + N_P, \qquad (4)$$

where N is the concentration of vanadium oxide in the sample. Substituting Eq. (2) into (4) yields

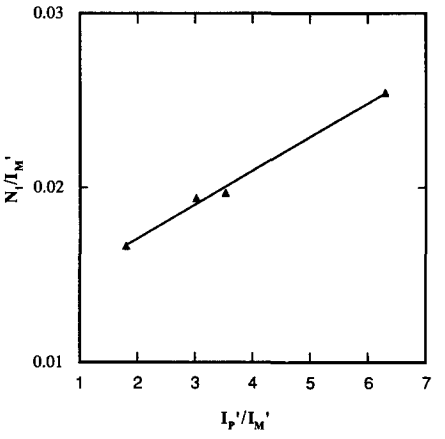

FIG. 4. Plot of N_i/I'_M versus I'_P/I'_M.

$$N = \frac{I'_M}{\sigma'_M} + \frac{I'_P}{\sigma'_P}, \qquad (5)$$

which after division by I'_M reduces to

$$\frac{N}{I'_M} = \frac{1}{\sigma'_M} + \frac{I'_P}{I'_M} = \frac{1}{\sigma'_P}. \qquad (6)$$

Figure 4 shows a plot of N/I'_M versus I'_P/I'_M, using the values reported in Table 3. Values for I'_M and I'_P were obtained by taking the area ratio of the peaks located at 1030 and 915–960 cm^{-1} (determined by Gaussian deconvolution) to the intensity of the TiO_2(a) peak at 520 cm^{-1}. Figure 4 shows that the experimental data are correlated by a straight line with an R^2 value of 0.994, indicating a very good fit. From the slope and intercept of this plot σ'_M and σ'_P are determined to be

$$\sigma'_M = 75 \frac{\text{rel. intensity}}{[M]\ (\text{g/g sample})}$$
$$\sigma'_P = 520 \frac{\text{rel. intensity}}{[P]\ (\text{g/g sample})}. \qquad (7)$$

The concentrations of monomeric and polymeric vanadia species in each sample were calculated from Eq. (2), using the values of σ'_M and σ'_P given above. A plot of the distribution of these species as a function of the V_2O_5 surface density is shown in Fig. 5.

TABLE 3

Quantitative Analysis of VO_x Species

Weight loading % V_2O_5	I'_M	I'_P	LRS[a]			TPO[b]		
			X_M	X_P	X_C	X_M	X_P	X_C
1.3	0.76	1.37	0.80	0.20	—	0.7	0.3	—
2.5	1.30	3.93	0.71	0.29	—	0.5	0.5	—
3.0	1.53	5.39	0.67	0.33	—	0.5	0.5	—
6.1	2.39	15.0	0.52	0.48	—	0.4	0.6	—
9.8	2.43	14.6	0.33	0.29	0.38	0.3	0.3	0.4

[a] Loading fraction for each species (M, monomer; P, polymer; C, crystallite), estimated error of ±7%.

[b] From integration of TPO profiles.

It is observed that with increasing vanadia loading, the fraction of vanadia present as monomeric species declines monotonically, while that present as polymeric species passes through a maximum. Also shown in Fig. 5 is the fraction of vanadia present as crystalline V_2O_5, calculated from the difference between the total vanadia and the dispersed (monomeric and polymeric) vanadia. The fraction of these species is zero for all but the highest loading sample (9.8% V_2O_5/TiO_2(a)). The formation of crystallites of V_2O_5 seems to occur at the expense of the polymeric species.

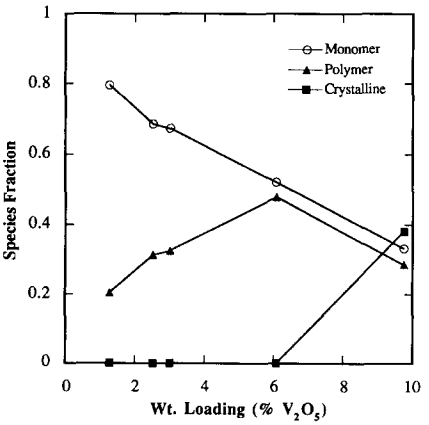

FIG. 5. The distribution of monomeric, polymeric, and crystalline V_2O_5 species as a function of the vanadium surface density. The estimated error in these quantities is ±7%, which is determined by the variance of the Gaussian fit from the data, and by the uncertainty in the vanadia loadings.

The behavior shown in Fig. 5 suggests that the distribution of vanadia species is governed by the following polymerization scheme

$$\begin{aligned} 2M &\rightleftarrows P_2 \\ M + P_2 &\rightleftarrows P_3 \\ &\vdots \\ &\vdots \\ nM &\rightleftarrows P_n, \end{aligned} \tag{8}$$

where M represent a monomeric species and P_n represents a polymeric species comprised of n vanadium centers. At equilibrium,

$$\ln [P_n] = \ln K_n - n \ln [M], \tag{9}$$

where $[P_n]$ is the concentration of polymeric species, $[M]$ is the concentration of monomeric species, n is the average polymer size, and K_n is the product of the equilibrium constants.

Figure 6 shows a plot of $\ln [P_n]$ versus $\ln [M]$. The slope of the curve fitted to the data has an average value of 2.4 over the range of V_2O_5 loadings. This suggests that the average number of vanadium atoms per polymeric species ranges from two to three.

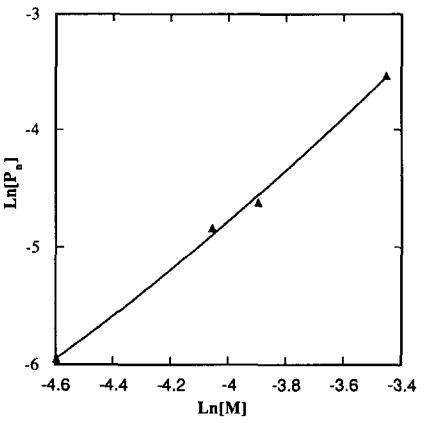

FIG. 6. A plot of ln $[P_n]$ versus ln $[M]$ used to estimate the average polymer length.

LRS: Reduced Catalysts

The structure of the TiO_2(a)-supported V_2O_5 catalysts was characterized following reduction in H_2 at elevated temperatures to determine the reducibility of the dispersed VO_x species. Raman spectra taken following reduction at temperatures from 523 to 623 K are presented in Figs. 7–9 for V_2O_5 loadings of 1.3, 6.1, and 9.8%, respectively. Each spectrum is normalized with respect to the TiO_2(a) peak at 520 cm^{-1}. For the 1.3% V_2O_5/TiO_2(a) sample, Fig. 7 shows that reduction at 523 K results in a slight decrease in intensity of both the band at 1030 cm^{-1} due to monomeric vanadyl species and the broad peak at 915 cm^{-1} due to the vibrations of terminal V=O bonds in polymeric species. In addition, the peak for the polymeric species shows a narrow component at 900 cm^{-1} which is not evident in the spectrum of the oxidized sample (Fig. 7a). Heating to 573 K reduces the intensity of the band at 1030 cm^{-1} and noticeably increases the intensity in the region from 750 to 850 cm^{-1}. In spectrum (d) taken at 623 K, the band at 1030 cm^{-1} has disappeared. A small peak remains at 900 cm^{-1}, but the majority of the spectral intensity is centered at 800 cm^{-1}. It is worth noting that no shift in position is observed for the monomeric peak located at 1030 cm^{-1}, indicating that water formed during reduction does not remain coordinated to this species (*7*, *9*).

The spectra recorded after H_2 reduction for the higher vanadia loadings display trends similar to those observed for the 1.3% V_2O_5/TiO_2(a) sample. However, more pronounced changes are detected in the polymeric species owing to the larger concentrations of these species at higher loadings. In the spectra shown in Fig. 8 for the 6.1% V_2O_5 loading, the peak at 1030 cm^{-1} decreases in intensity as the reduction temperature is raised. Exposure to H_2 at 523 K results in the disappearance of the narrow portion of the polyvanadate band at 960 cm^{-1}, as well as an increase in intensity in the 750–850 cm^{-1} region of the spectrum. Reduction of the polyvanadate species at 523 and 573 K results in the appearance of a peak at 910 cm^{-1}, similar to that observed for the 1.3% loading. Raising the temperature to 623 K continues the overall shift in intensity to lower wavenumbers, resulting ultimately in a broad peak centered at 800

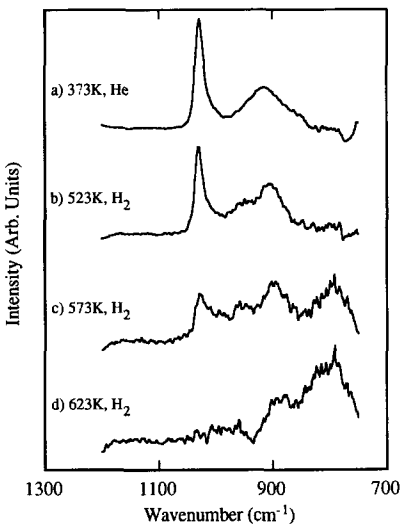

FIG. 7. Raman spectra of 1.3% V_2O_5/TiO_2(a) taken in dry H_2 at 383 K after reduction for 1 h at: (b) 523 K; (c) 573 K; (d) 623 K. Spectrum (a) taken at 373 K in He is shown for reference. Spectra are displayed following background subtraction over the region of 700–1200 cm^{-1}.

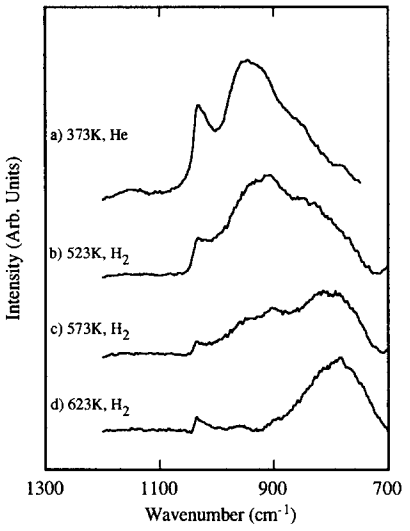

FIG. 8. Raman spectra of 6.1% V_2O_5/TiO_2(a) taken in dry H_2 at 383 K after reduction for 1 h at: (b) 523 K; (c) 573 K; (d) 623 K. Spectrum (a) taken at 373 K in He is shown for reference. Spectra are displayed following background subtraction over the region of 700–1200 cm^{-1}.

cm^{-1}. Similar behavior is seen in Fig. 9 for the 9.8% loading. As was the case for the 6.1% V_2O_5/TiO_2(a) sample, mild reduction at 523 K results in the suppression of the polyvanadate band at 960 cm^{-1}, attributed to vanadyl groups within the polymeric species. A slight decrease in the bands due to crystalline V_2O_5 (997 cm^{-1}) and monomeric species (1030 cm^{-1}) are also seen in Fig. 9b, along with an increase in intensity in the region from 750 to 900 cm^{-1}. After reduction at 573 K, only a small peak remains at 997 cm^{-1}, due to crystalline V_2O_5. Several other Raman peaks are seen in spectrum (c) of Fig. 9. These features are all weak and are located at 1030, 960, and 910 cm^{-1}. An intense broadband extending from 750 to 900 cm^{-1} is also observed. Elevating the reduction temperature to 623 K results in a Raman spectrum in which the only discernable features are a small band at 1030 cm^{-1} and a broad peak at 800 cm^{-1}.

New features are observed in the Raman spectra recorded following the reduction of TiO_2(a)-supported V_2O_5 that are not evident in the spectra of the oxidized samples. After mild reduction treatments at 523 and 573 K, all of the samples exhibit a narrow feature at ~910 cm^{-1}. The intensity of this peak decreases, though, when reduction is carried out at 623 K. As it is present at all loadings, it is safe to assume that this peak is not associated with the crystalline species which are only observed in the spectra of 9.8% V_2O_5/TiO_2(a) sample (Fig. 9). The intensity of the peak at ~910 cm^{-1} is also unrelated to the presence or absence of the peak at 1030 cm^{-1} due to monomeric species. The peak at 910 cm^{-1} is also observed in the spectrum of 6.1% V_2O_5/TiO_2(a) taken at 673 K in He (*20*), which rules out its assignment to any species formed by hydroxylation or by adsorption of water during reduction. Taken together, these observations suggest that the band at 910 cm^{-1} arises from the vanadyl group of a partially reduced polyvanadate species, though conclusive assignment by comparison with Ra-

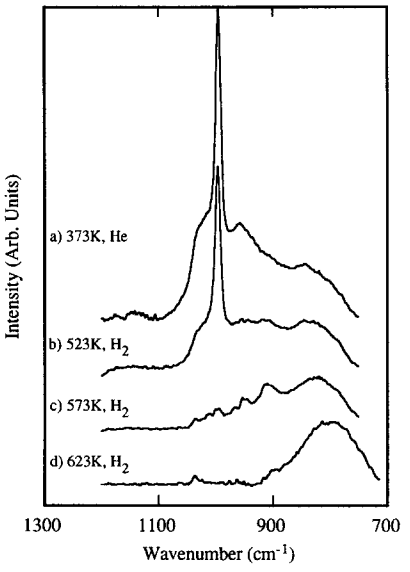

FIG. 9. Raman spectra of 9.8% V_2O_5/TiO_2(a) taken in dry H_2 at 383 K after reduction for 1 h at: (b) 523 K; (c) 573 K; (d) 623 K. Spectrum (a) taken at 373 K in He is shown for reference. Spectra are displayed following background subtraction over the region of 700–1200 cm^{-1}.

man spectra of model compounds cannot be made at this time.

The reduction of the dispersed VO_x species is accompanied by a gradual shift in spectral intensity from the region of 900–1000 cm^{-1} to the region of 700–900 cm^{-1}. After reduction at 623 K, all of the intensity is located in this latter region. Prior to H_2 reduction, the only peak in the 700–900 cm^{-1} region is located at 840 cm^{-1}, attributed to the V–O–V bending vibrations in polyvanadate species. The intensity of the peak at 840 cm^{-1} is unchanged following reduction of both the 9.8 and 6.1% samples at 523 K, whereas the intensity associated with V=O terminal vibrations decreases sharply. These observations indicate that the terminal oxygen atoms of the polyvanadates are more susceptible to attack by hydrogen than the bridging oxygens. Elevating the reduction temperature to 623 K leads to the disappearance of the band associated with the V=O groups in oxidized polyvanadates and the appearance of a broad feature centered at 800 cm^{-1}. The position of this remaining feature, combined with the TPR results discussed below, suggests that the 800 cm^{-1} peak arises from V^{3+}=O groups, which remain in the polyvanadate species after reduction at 623 K. This assignment is supported by the observation that the V=O bond length of oxovanadium compounds increases as the oxidation state of vanadium decreases (*21*). Spectra recorded after reoxidation of the reduced samples are identical to those observed for the freshly calcined samples shown in spectrum (a) of Figs. 7–9, indicating that the reduction/reoxidation process is fully reversible.

Temperature-Programmed Reduction/Oxidation

The integrated amounts of H_2 consumed during TPR, and of O_2 consumed during TPO, are listed in Table 4. For each sample, the ratios of H_2/V and O/V are nearly unity, in good agreement with previous studies that show that V^{5+} species are reduced to V^{3+} without significant reduction of the TiO_2 (*13, 22, 23*). Significant water evolution was observed during the TPR experiments, but hardly any water was detected during TPO. This indicates that water formed during TPR desorbs and that hydrogen atoms do not remain on the surface of the catalyst following reduction. The source of the oxygen involved in the reduction and reoxidation of the dispersed vanadia is suggested by the Raman spectra presented in Figs. 7–9. As discussed above, these spectra suggest that the terminal oxygens of the monomeric and polymeric species are much more labile (with regard to reduction by H_2) than the V–O–V bridging oxygens of the polymers. Taken together, these observations suggest the occurrence of the following processes during TPR and TPO:

Monomeric vanadyls:

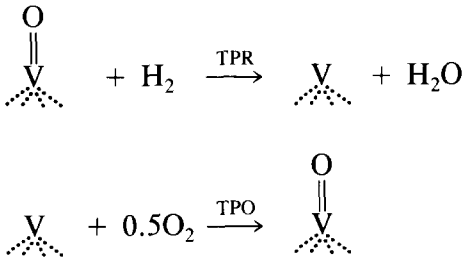

Polymeric vanadates:

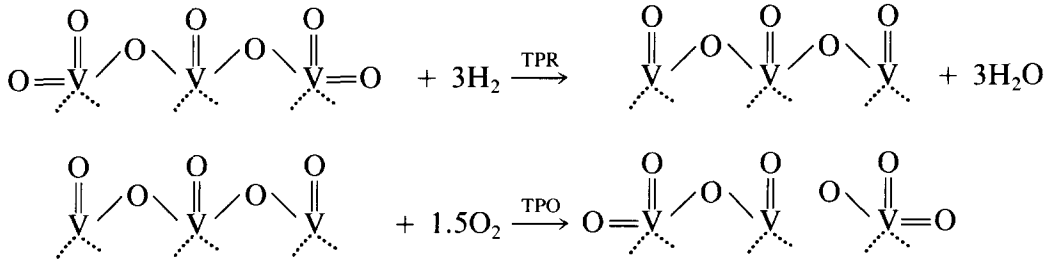

TABLE 4

Calculated H_2 and O_2 consumptions during TPR and TPO[a]

Weight loading % V_2O_5	TPR H_2/V	TPO O/V
1.3	1.2	1.0
2.5	1.1	0.9
3.0	1.2	0.9
6.1	1.1	1.0
9.8	1.2	1.0

[a] From integration of TPR and TPO profiles, estimated error of ±10%.

In each of these schemes, the structure on the left-hand side represents the state of the dispersed species at the start of TPR or TPO, and the structure on the right-hand side represents the state of the dispersed species at the end of TPR or TPO.

While the above schemes show reduction only of the terminal vanadyl oxygens, it is conceivable that the oxygen atoms bonding the VO_x species to the support also undergo reaction with hydrogen as well. Thus, for example, the reduction of monomeric vanadyls can be envisioned to proceed via the following steps:

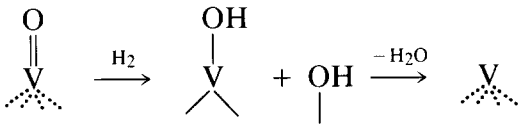

Several pieces of evidence support such a sequential reduction process. First, it is observed that the consumption of H_2 during TPR starts at 350 K, whereas the appearance of H_2O does not begin until 425 K. Second, Raman studies of NH_3 reduction of the samples used in the present study show clear evidence for the formatin of hydroxyl groups associated with both the support and the dispersed vanadia (*20b*) and ^1H NMR observations of adsorbed NH_3 (*24*) show definitive evidence for NH_4^+ cations formed by the reaction of NH_3 groups on the vanadia. Third, CO_2 adsorption on partially reduced V_2O_5/Al_2O_3 produces bicarbonte species via the reaction of CO_2 with surface -OH groups (*25*).

Efforts to resolve differences in the TPR profiles associated with the reduction of the individual VO_x species were not successful; however, separate peaks were observed in the TPO profiles, as can be seen in Fig. 10. For the 1.3% V_2O_5/TiO_2(a) sample, the TPO profile consists of a ~100 K wide peak at 530 K superimposed on a broad peak extending from 350 to 773 K. The narrow feature remains at 530 K as the V_2O_5 loading is increased to 3.0%, but the contribution of the underlying peak to the overall area increases. Increasing the V_2O_5 loading to 6.1% results in a shift of the peak at 530 K to 550 K and a continued increase in the fraction of the total area contributed by the broad peak. By contrast to the other samples, the 9.8% V_2O_5/TiO_2(a) sample exhibits a high-temperature peak at 720 K, in addition to a peak centered at 580 K, and a broad peak underlying these features extending from 350 to 773 K.

The differences observed in the reoxidation profiles shown in Fig. 10 as the V_2O_5

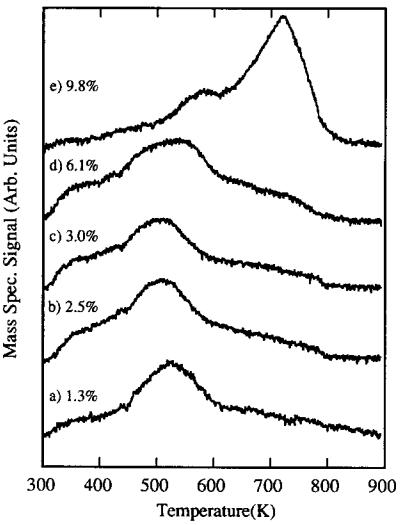

FIG. 10. Temperature-programmed oxidation profiles for: (a) 1.3% V_2O_5/TiO_2(a); (b) 2.5% V_2O_5/TiO_2(a); (c) 3.0% V_2O_5/TiO_2(a); (d) 6.1% V_2O_5/TiO_2(a); and (e) 9.8% V_2O_5/TiO_2(a). Profiles obtained following reduction in H_2 at 773 K for 1 h.

loading is increased from 1.3 to 9.8% provide additional information regarding the structure and reduction/reoxidation behavior of the dispersed V_2O_5. The peak at ca. 530–580 K is attributed to the reoxidation of the monomeric species because the intensity of this feature decreases relative to that of the underlying peak extending from 350 to 773 K as the V_2O_5 loading increases from 1.3 to 6.1%. This interpretation is consistent with changes in the relative intensity of the Raman features reported in Fig. 1. The broad peak observed at all loadings is attributed to the polymeric vanadates, which are likely to exhibit a broader distribution of structures and, hence, a broader spectrum of oxidation temperatures. The peak at 720 K observed in the TPO profile of the 9.8% V_2O_5/TiO_2(a) sample is attributable to the reoxidation of crystalline V_2O_5. This interpretation is consistent with the observation that crystallites of V_2O_5 are detected only in the Raman spectrum of the 9.8% V_2O_5/TiO_2(a) sample (see Fig. 1).

Integration of the areas of the separate TPO peaks in Fig. 10 provides support for the quantities of each species determined by Raman spectroscopy. Because the peak shapes are not well defined, it is difficult to assess the areas of overlapping TPO features. The approach taken here is to ascribe the area above a line extending from 350 to 725 K to the monomeric species, the area below this line and above the horizontal background to the polymeric vanadates, and the narrow 720 K peak in the profile of the 9.8% V_2O_5/TiO_2(a) to crystallites of V_2O_5. The results of these calculations are presented in Table 3. Good agreement is seen between the distributions of vanadia species estimated from TPO and Raman spectroscopy for the 9.8% V_2O_5/TiO_2(a) sample, for which the TPO peaks are reasonably well resolved. As the loading decreases, the overlap between the TPO peaks makes their resolution difficult. Nevertheless, qualitative agreement between the two methods for calculating the distribution of vanadia species is observed.

The combination of TPR/TPO and LRS experiments indicates that a maximum of one terminal oxygen atom per vanadium is removed during reduction at temperatures up to 773 K. Subsequent reoxidation restores the oxygen removed by reduction. These experiments support the use of oxygen chemisorption as a method for determining the dispersion of supported V_2O_5 catalysts (*9, 14*). The distribution of monomeric, polymeric, and crystalline vanadia species determined in this study will be used to interpret the results of experiments examining the adsorptive and catalytic properties of V_2O_5/TiO_2(a) (*20*).

CONCLUSIONS

In situ Raman spectroscopy indicates that V_2O_5/TiO_2(a) catalysts contain monomeric vanadyl and polymeric vanadate species, as well as crystallites of V_2O_5. Quantitative analysis of the Raman spectra shows that monomeric species predominate at low vanadia loadings and then react to form polymeric vanadates as the loading increases. Crystallites of V_2O_5 form at the expense of the polymeric species if the vanadia loading increases above the dispersive capacity of the TiO_2(a) support. Analysis of the concentrations versus vanadia loading shows that the average polymer size is two at a loading of 1.3% V_2O_5 and increases to three as the loading increases to 9.8% V_2O_5. Upon reduction in H_2, Raman spectroscopy reveals that oxygen atoms from terminal V=O groups associated with monomeric and polymeric species are removed preferentially to V–O–V bridging oxygens. TPR and TPO experiments confirm that only one oxygen atom per vanadium is involved in the reduction/reoxidation process.

ACKNOWLEDGMENTS

This work was supported by the Director, Office of Energy Research, Office of Basic Energy Sciences, Chemical Sciences Division of the U.S. Department of Energy under Contract No. DE-AC03-76SF00098. We thank Marjorie S. Went and Heather Rumsey for preparing and characterizing the samples.

REFERENCES

1. Bauerle, G. L., Wu, S. C., and Nobe, K., *Ind. Eng. Chem Prod. Res. Dev.* **17,** 117 (1978).
2. Shikada, T., Fujimoto, K., Kunugi, T., Tominaga, H., Kaneko, S., and Kubo, Y., *Ind. Eng. Chem. Prod. Res. Dev.* **20,** 91 (1981).
3. Pearson, I. M., Ryu, H., Wong, W. C., and Nobe, K., *Ind. Eng. Chem Prod. Res. Dev.* **22,** 381 (1983).
4. Bond, G. C., and Bruckman, K., *Faraday Discuss. Chem. Soc.* **72,** 235 (1982).
5. Gasior, M., Gasior, I., and Grzybowska, B., *Appl. Catal.* **10,** 87 (1984).
6. Wachs, I. E., Saleh, R. Y., Chan, S. S., and Cherisch, C. C., *Appl. Catal.* **15,** 339 (1985).
7. Cristiani, C., Forzatti, P., and Busca, G., *J. Catal.* **116,** 586 (1989).
8. Busca, G., *Mater. Chem. Phys.* **19,** 157 (1988).
9. Went, G. T., Oyama, S. T., and Bell, A. T., *J. Phys. Chem.* **94,** 4240 (1990).
10. Machej, T., Haber, J., Turek, A. M., and Wachs, I. E., *Appl. Catal.* **70,** 115 (1991).
11. Eckert, H., and Wachs, I. E., *J. Phys. Chem.* **93,** 6796 (1989).
12. (a) Griffith, W. P., and Wickins, T. D., *J. Chem. Soc. A* 1087 (1966); (b) Griffith, W. P., and Lesniak, P. J. B., *J. Chem. Soc. A* 1066 (1969).
13. Roozeboom, F., Mittelmeijer-Hazeleger, M. C., Moulijn, J. A., Medema, J., de Beer, V. H. J., and Gellings, P. J., *J. Phys. Chem.* **84,** 2783 (1980).
14. Oyama, S. T., Went, G. T., Lewis, K. B., Bell, A. T., and Somorjai, G. A., *J. Phys. Chem.* **93,** 6786 (1989).
15. Abello, L., Husson, E., Repelin, Y., and Lucazeau, G., *Spectrochim. Acta A* **39,** 641 (1983).
16. (a) Selig, H., and Claassen, H. H., *J. Chem. Phys.* **44,** 1404 (1966); (b) Miller, F. A., and Cousins, L. R., *J. Chem. Phys.* **26,** 329 (1957); (c) Miller, F. A., and Baer, W. K., *Spectrochim. Acta* **17,** 112 (1961).
17. Boehm, H. P., *in* "Advances in Catalysis" (D. D. Eley, H. Pines, and P. B. Weisz, Eds.), Vol. 16, p. 249. Academic Press, New York, 1966.
18. Calomon, H. J., Hirota, E., Kuchitsu, K., Lafferty, W. J., Maki, A. G., and Pote, C. S., *in* "Structure Data of Free Polyatomic Molecules," New Series, Group II, Vol. 6. Landolt-Borstein, Berlin, 1976.
19. Griffith, W. P., and Wickins, T. P., *J. Chem. Soc. A,* 404 (1968).
20. (a) Went, G. T., Leu, L.-J., Rosin, R. R., and Bell, A. T., *J. Catal.* **134,** 492 (1992); (b) Went, G. T., Leu, L.-J., Lombardo, S. J., and Bell, A. T., *J. Phys. Chem.*, in press.
21. Sieblin, J., *Coord. Chem. Rev.* **1,** 293 (1966).
22. Bond, G. C., Zurita, J. P., Flamerz, S., Gellings, P. J., Bosch, H., Van Ommen, J. G., and Kip, B. J., *Appl. Catal.* **22,** 361 (1986).
23. Haber, J., Kozlowska, A., and Kozłowski, R., *J. Catal.* **102,** 52 (1986).
24. M. T. Went, Ph.D. thesis, Department of Chemical Engineering, University of California, Berkeley, CA, 1991.
25. Sobalik, Z., Kozłowski, R., and Haber, J., *J. Catal.* **127,** 665 (1991).